A Computational Workflow to Determine Saddle Position Effects on Metabolic Energy Expenditure Rate While Cycling

ME 329 2021: Specialized Team

18 March 2021

C. Chen, C. Clancy, D. Gonzalez, S. Rostamzadeh

Index

Introduction

Cycling is a popular activity for both recreational and elite athletes, and the bicycle is referred to by many as the most efficient mode of transportation[3]. As with other forms of movement, cycling has been studied extensively in the world of biomechanics. Cycling research consists of multidisciplinary efforts from mechanical engineering, physiology, kinesiology, and sports medicine for applications in athletic efficiency, physical therapy, and injury prevention[11][16][21][25]. Extensive research has been performed investigating how cycling efficiency is affected by various changes in cycling dynamics, such as changes in muscle activation[16], pedaling cadence[18], cycling shoe placement[7], or a combination of these factors, which have been shown to be interrelated[2][9][11][12][17].

Quantitatively, efficiency is defined as the ratio of mechanical power output at the bicycle wheels to the metabolic energy expenditure rate of the rider[30]. Metabolic energy expenditure rate, or MEER, is defined as the metabolic power consumed by the muscles (measured in Watts) and is calculated as the rate at which heat is released plus the rate at which work is performed by the muscles[20][29]. The total MEER is proportional to the sum of the resting MEER and the ATP consumption rate of each muscle, the conversion of chemical to mechanical power[40]. MEER is a metric that biomechanical engineers use to quantify the extent to which some movement is efficient and is typically measured experimentally through gas exchange via indirect calorimetry, which measures oxygen consumption during exertion[21]. When applied to research on cycling dynamics, MEER is often minimized as researchers try to maximize theoretical rider efficiency. Many research groups have investigated MEER in other forms of movement, such as running or walking, through musculoskeletal modeling with the computational biomechanics research software package OpenSim[4][5][6][7][13][14][15].

Related Work

OpenSim has been extensively used in research and industry as a biomechanics modeling tool to model musculoskeletal dynamics. In 2007, Dr. Scott Delp and his team at Stanford first released the software to the world as an open-source tool. Delp's research group at Stanford has published several papers regarding MEER, mostly using their robust walking models. Their 2017 study showed how OpenSim can be used to simulate ideal assistive walking devices with the goal of reducing MEER[5]. The software's built-in Forward Dynamics Tool solves for kinematics and kinetics based on prescribed initial conditions[41]. The software's built-in Computed Muscle Control (CMC) Tool solves for the model's muscle activations for a given motion and can output MEER results[42]. Several other Stanford publications related to the MEER of walking and running heavily focused on results from OpenSim's CMC Tool[13][14][15]. Some researchers outside of Delp's group have published literature using OpenSim centered on cycling mechanics. In 2008, a master's student from Ball State University modified a preexisting two-legged OpenSim model to represent a cycling motion in order to determine MEER as a function of cycling shoe, or cleat, placement on the pedal[7].

Many researchers have analyzed how various changes in cycling dynamics affect cycling efficiency. One group of researchers investigated how cycling is affected by the hip joint angle, the angle formed between the lines of the torso and the thigh. They showed that changing the hip joint angle affects MEER, power output, muscle activation, and overall body kinematics[2]. Furthermore, experimental research studies have been performed to measure muscle activation and joint angles while cycling[16][17][18]. It is important to note that the data from these studies was professionally extracted from a series of empirical trials with expert cyclists, utilizing electromyography (EMG) to measure muscle excitation and 3D motion capture technology to measure joint angles.

Biomechanics Analysis: Muscle States

Muscle states are the muscle fiber lengths and muscle fiber velocities (speed of contraction) for a particular muscle at a moment in time and provide valuable insights regarding how MEER is minimized without explicitly calculating MEER itself. The active force a muscle is capable of generating is based on the muscle force-length and force-velocity relationships. The force-length relationship in muscle is seen in **Figure 1**. The muscle fiber length is normalized by the optimal fiber length, which is defined as the fiber length at which maximum active muscle force is achieved. The muscle fiber force is normalized by the maximum isometric force, F_O^M, which is the muscle force at optimal fiber length. The passive force generated by a muscle is also normalized by the maximum isometric force and is plotted against the muscle fiber length.

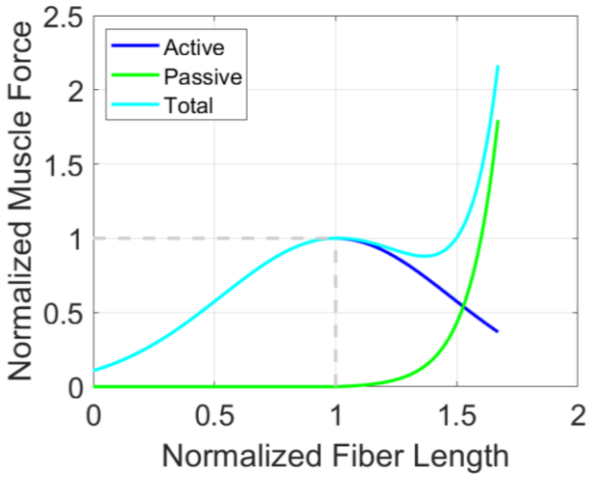

***Figure 1**, The force-length curves for active muscle force, $f^L(l^M)$, and passive muscle force, $f^{PE}(l^M)$. The muscle fiber velocity is assumed to be zero (isometric contraction). The curves were plotted using the equation for $f^L(l^M)$ and $f^{PE}(l^M)$ as defined in OpenSim source code[43][44].*

The force-velocity relationship for muscle fibers is defined only for active force and is seen in **Figure 2**. Concentric contractions correspond to a shortening of the muscle, and eccentric contractions correspond to a lengthening of the muscle. When a muscle concentrically contracts, it performs positive mechanical work. This is relevant to our study as this behavior can be used to identify the active force capacity a muscle can generate[43][44].

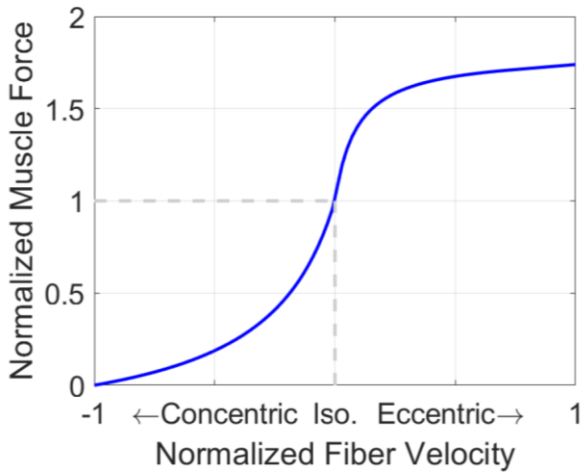

***Figure 2**, The force-velocity curve for active muscle force, $f^V(v^M)$. The muscle fiber length is assumed to be at the optimal fiber length, with only fiber velocity varying as the muscle contracts and lengthens. The curve was plotted using the equation for $f^V(v^M)$ as defined in OpenSim source code[43][44].*

The active force capacity of a muscle is a combination of the active muscle force from the active force-length and force-velocity relationships. The active force that a muscle exerts is also dependent on an activation value, *a*, which is a fraction representative of how many muscle fibers of a whole muscle are recruited. This active force plus the passive force of a muscle yields the total muscle force. **Equation (1)** calculates the force produced by a muscle based on muscle activation and muscle states[21]. A main takeaway from **Equation (1)** is that the activation is not a function of the force from the muscle length and muscle velocity.

$$F^M(t) = F_o^M[a(t)\, f^L(\ell^M(t))\, f^V(v^M(t)) + f^{PE}(\ell^M(t))] \quad \textbf{(1)}$$

$F^M(t)$ = total muscle force
F_O^M = maximum isometric force
$a(t)$ = muscle activation $\in [0, 1]$
$f^L(l^M(t))$ = normalized active force due to normalized muscle fiber length
$f^V(v^M(t))$ = normalized active force due to normalized muscle fiber velocity

$f^{PE}(l^M(t))$ = normalized passive force due to normalized muscle fiber length

The active force capacity of a muscle is based on the muscle state as it is the product of the force due to the muscle length, $f^L(l^M(t))$, and the force due to the muscle velocity, $f^V(v^M(t))$, as seen in **Equation (1)**. If a muscle has a higher active force capacity due to its muscle states, the muscle will require less activation to generate the same amount of force [21]. So, with a larger active force capacity, less activation will be required to generate a given motion and the MEER will be smaller than when compared to a muscle performing the same motion with a lower active force capacity. Thus, one can use **Equation (1)** to determine valuable insights about MEER without calculating MEER.

Research has been performed linking these muscle states and MEER in human movement. Both Sebastian Bohm and Julian Alcazar's research groups proved that these force-length and force-velocity relationships are highly correlated to MEER based on experimental testing[22][23]. These studies paved the way for analysis of MEER in human movement guided by muscle states. Furthermore, Brian Umberger and his team used these muscle states in developing and validating a comprehensive human MEER model with the intention that this model could be used with computer models[24]. Umberger's modeling of MEER was incorporated into the OpenSim Application Programming Interface (API)[20], which was used in this project to determine how seat position was related to MEER in cycling.

Problem Context

Our industry partner, Specialized, investigates how to make the most efficient mode of transportation more efficient[1]. MEER is a main indicator of efficiency, and therefore, one area of interest in cycling efficiency research is investigating how changing the bicycle saddle (seat) position affects MEER. Traditional methods of sport performance analysis perform subject-specific measurements in a lab, such as motion capture and force data, to create subject-specific models[9][10][11][12][16][17][18][21]. This is often a lengthy process and takes years to complete. We seek to expedite this process by establishing purely computational methods to enable Specialized to streamline their design cycle. Our goal is to establish a workflow to quantify the relationship between MEER and saddle position using modeling with OpenSim and subsequent analysis. Specialized will then be able to incorporate this computational workflow framework from our OpenSim simulations into their bicycle design cycle to make design changes that maximize cycling efficiency for elite riders.

Problem Definition

The position of the saddle of the bicycle can be adjusted to tune for cycling performance. It is postulated that changing the saddle position of a bicycle can affect the MEER of the cyclist and that a saddle position can be found to minimize MEER[10][25][26]. The position of the saddle is defined by the seat tube height, R, and seat tube angle, θ, as seen in **Figure 3**.

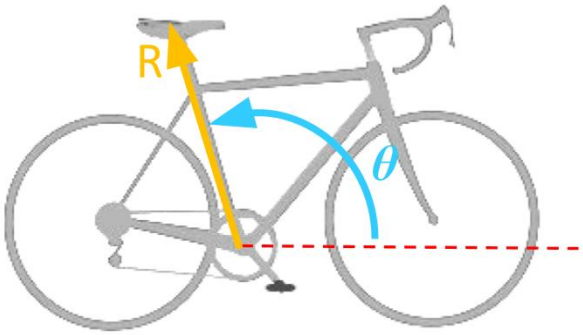

***Figure 3**, Definition of saddle position (R, θ). Saddle position was defined as a function of the seat tube height, R, the distance between the bottom bracket and the saddle, and the seat tube angle, θ, the angle between the positive horizontal axis and vector from bottom bracket to the saddle[30].*

This project sought to create a computational workflow method with OpenSim and subsequent

analysis to relate saddle position and MEER. This could be applied in the future to determine the saddle position(s) for elite cyclists aiming to maximize their cycling efficiency by minimizing their MEER. This workflow was created by leveraging the Forward Dynamics and Computed Muscle Control (CMC) Tools of OpenSim.

To prove our workflow a viable method, we generated and analyzed results for a complete workflow and analysis cycle. We analyzed the effects of changing saddle position (R, θ as the parameterized inputs) on MEER (as the output) in OpenSim. We used a simplified musculoskeletal model to determine the dynamics and MEER for different saddle positions for a set, constant pedaling cadence of 80 revolutions per minute (RPM). The 80 RPM value was chosen as it was the average cadence analyzed in literature[11], while a constant cadence was chosen as it was validated by literature[31] and data provided by Specialized[32].

Methods

Model

Our team leveraged an existing, simplified musculoskeletal model from the 2018 ME485 project course (Modeling and Simulation of Human Movement) at Stanford[19] as a starting point to which we added complexity to more adequately address our particular research problem. The inherited model was a simple model, with only four muscles in the upper leg (i.e. no musculature below the knee), fixed foot-to-pedal constraints, and a fixed pelvis location. The ME485 group was able to run a forward-dynamics-based simulation, but the cycling motion was driven solely by the assumed, prescribed activation of one muscle. Our team used this model as a starting point to develop a full workflow methodology that outputted more realistic cycling kinematics, dynamics, and the capability of calculating MEER.

Model Degrees of Freedom & Constraints

The model consisted of 13 degrees of freedom (DOF), also known as “coordinates” in OpenSim. The model DOF included the crank angle, pelvis x-direction translation, pelvis y-direction translation, pelvis z-direction translation, pelvis list angle, pelvis rotation angle, pelvis tilt angle, hip adduction angle, hip rotation angle, hip angle, knee angle, ankle angle, and metatarsophalangeal (MTP) angle. Diagrams of each DOF are found in **Appendix A**.

The pelvis translational DOF (pelvis x-direction translation, pelvis y-direction translation, pelvis z-direction translation) and rotational DOF (pelvis list angle, pelvis rotation angle, pelvis tilt angle) were fixed for the subsequent analyses. This represented the fixed position of the cyclist on the saddle.

The remaining six free DOF of the model (hip adduction angle, hip rotation angle, hip angle, knee angle, ankle angle, MTP angle) were bounded between a minimum and a maximum value based on physiological limits. For example, the knee angle was bounded between -180° and -22°.

The model had a Weld Constraint (full translational and rotational coupling) between the pedal and the midfoot. This represented a clipped-in, cycling shoe-to-pedal interface and will be referred to as the pedal clip constraint.

The OpenSim Multi-Body dynamics solver code contains optimization calculations to relate the joint angles through their trajectories and to satisfy the imposed holonomic constraints on the model. For example, in the first step of our workflow, Simulated Forward Kinematics, a prescribed input was given to the crank angle as a function of time. As the crank angle moved through its trajectory, at intermediate time steps, the OpenSim Multi-Body dynamics solver code found nearby positions for the six free DOF that satisfied the new time step holonomic constraints and the fixed DOF constraints with an optimization (see

Appendix B for the optimization equation). This optimization is not stochastic and given the same initial conditions and constraints, the solver will reproduce the same motion for a model [34][35][37]. The initial conditions prescribed to the model will be described in the following subsection.

Forward Dynamics Tool

The software's built-in Forward Dynamics Tool generated model coordinate kinematics and kinetics based on prescribed initial conditions. When the Forward Dynamics Tool in OpenSim was used to run a simulation, a new set of coordinates for the model needed to be solved for at every time step of the simulation (see **Appendix B**). Each time step's set of coordinates was not allowed to violate the imposed DOF constraints on the model.

The Forward Dynamics Tool determines the motion of a model given the model's initial position and constraints on DOF. External forces or prescribed functions in time on DOF drive the model's motion. The outputs of the Forward Dynamics Tool relevant to this study are joint angles, muscle fiber lengths, muscle fiber velocities, and reaction forces due to model constraints.

Computed Muscle Control (CMC) Tool

The Computed Muscle Control (CMC) Tool performs an algorithm that solves for the muscle activations that are required by the model to generate a user-specified, desired motion. The muscle activations are chosen by the CMC Tool such that an objective function, J, equal to the squared sum of muscle activations and the squared sum of errors of joint angle accelerations, is minimized, as seen in **Equation (2)** [42].

$$J = \Sigma w_i x_i^2 + \Sigma w_j (q''_{j,\,des} - q''_{j,\,CMC})^2 \quad \textbf{(2)}$$

w_i = *weights on model controls*
x_i = *actuator controls* $\in [0, 1]$
w_j = *weights on coordinate deviations*
$q''_{j,\,des}$ = *desired coordinate accelerations*
$q''_{j,\,CMC}$ = *current coordinate accelerations for the model during CMC simulation*

The weights of the acceleration deviations are referred to as "tracking tasks" in OpenSim. Not all of the coordinates of the model need to be "tracked" via weights in order to use the CMC Tool. This allows for simplification of the optimization problem by only considering a minimal subset of DOF for the desired coordinate accelerations. "Actuators" of the model consist of all of the muscles included in the model plus OpenSim "reserve actuators", which are specified by the user. Reserve actuators apply the minimum amount of torque to the joints that is needed to drive the motion specified by the desired coordinates when there is too little musculature or the muscles are not strong enough.

Workflow

The workflow we developed was entirely computational and did not rely on experimental data collection. The first step of the workflow, Simulated Forward Kinematics (SFK), substituted the traditional step of motion capture measurements and pedal reaction force data collection. The second step of the workflow, Computed Muscle Control (CMC), used the results from the SFK step to make muscle activation calculations that would ultimately allow MEER results to be calculated and analyzed.

Workflow Inputs

The parameterized input for our model was the saddle position of the bicycle with respect to the bottom bracket. The global x- and y-coordinates of the pelvis location were calculated from a seat tube angle, θ, and seat tube height, R, from the bottom bracket. To choose R, we measured the inseam leg length of the OpenSim model. Inseam leg length was defined as the distance from the pubic bone to the floor while in standing posture at full knee extension[25]. From literature, we implemented the LeMond method for calculating seat tube height from inseam leg length[25]. This method is derived from Tour de France champion, Greg LeMond's preferred seat tube height, and places the seat tube height at 88.3% of inseam length[25]. After calculating the new seat tube height, the seat tube

angle range was obtained from literature[46]. **Figure 4** shows how the angle and heights were varied for the different trials. We chose three seat tube angles: θ = {102°, 105°, 108°}, and two seat tube heights: R = {0.8196 m, 0.8396 m}, giving us six unique saddle positions for our investigation.

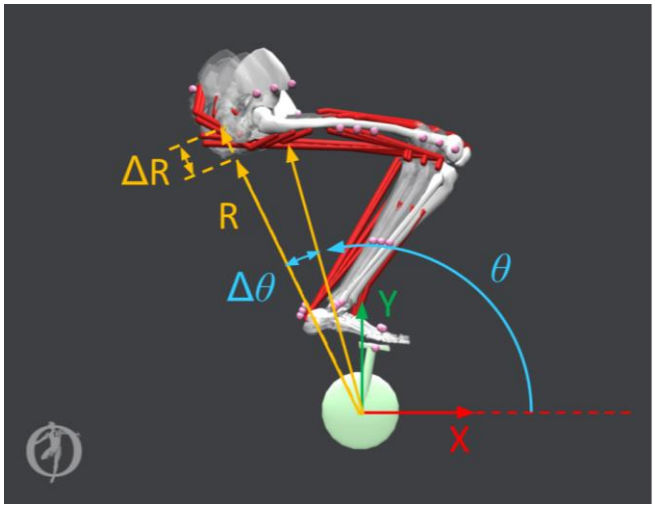

***Figure 4**, Overlay of models used for the various trials by varying the seat tube angle and seat tube height. The x- and y-coordinates for the saddle position were computed using a set of polar coordinates, radius, R, for seat tube height and angle, θ, for seat tube angle. 6 unique saddle positions were investigated for θ = {102°, 105°, 108°} and R = {0.8196 m, 0.8396 m}.*

Simulated Forward Kinematics (SFK)

The Simulated Forward Kinematics (SFK) step of the workflow was where the model leg passively followed a cycling motion, and the motion and reaction force data for the leg was extracted for later analysis. This step substituted data normally collected from motion capture experiments where joint angles of a subject would be recorded as the subject performed some motion, and external reaction forces would be measured from force plates. This was achieved by prescribing a constant velocity function to the crank angle of the model, and then the model passively followed the crank via the pedal clip constraint.

The key outputs of the SFK trials were joint angles, muscle fiber lengths, muscle fiber velocities, and reaction pedal forces at the midfoot, all as functions of time, as seen in **Figure 5**.

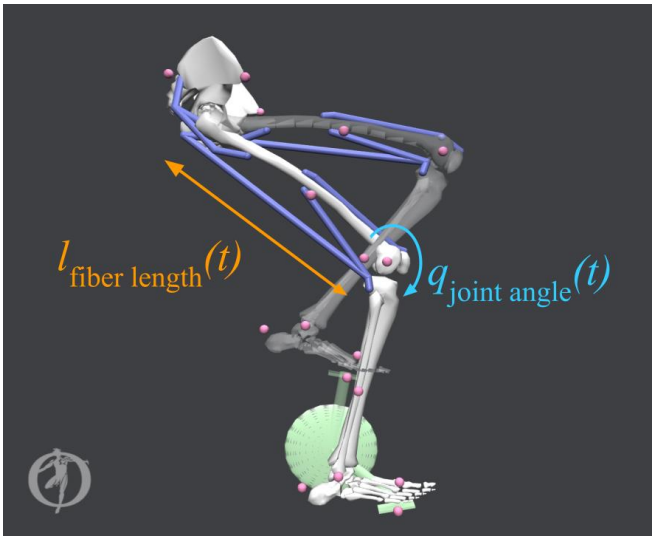

***Figure 5**, Outputs of Simulated Forward Kinematics (SFK) step. As the model leg passively followed a constant-cadence turned crank, data was outputted as functions of time for the model joint angles, muscle fiber lengths, muscle fiber velocities, and pedal reaction forces at the midfoot. The labels show the changing joint angle at the knee joint and the changing muscle fiber length of the biceps femoris long head.*

The data of the muscle fiber lengths and muscle fiber velocities, the muscle states of the model, were later used to compute the active force capacity of all muscles at any given time during the SFK simulation. The SFK trial outputs, specifically, kinematics of the DOF and external forces at the pedal clip constraint, were then used as inputs to the subsequent corresponding CMC trial.

The pedal clip constraint imposed forces on the midfoot during the SFK trials. We treated this reaction force as a first order approximation for pedaling resistance magnitude. The pedal reaction forces were smoothed using “rloess” smoothing in MATLAB. This is a quadratic regression-based smoothing with further adjustments to filter outliers, and was implemented with a window size of 50 data points. The data for the smoothed forces were written to a file to be used with the subsequent corresponding CMC trial.

Computed Muscle Control (CMC)

The Computed Muscle Control (CMC) step of our workflow took in inputs of kinematics and smoothed reaction forces from the SFK stop and generated a set of muscle activations that, when applied to the model muscles, produced the same motion as found in the SFK step. The CMC Tool ran a simulation, and at every time step, a set of muscle activations were solved via minimization of the optimization function (shown in **Equation (2)**) that moved the model forward in time, shown in **Figure 6**.

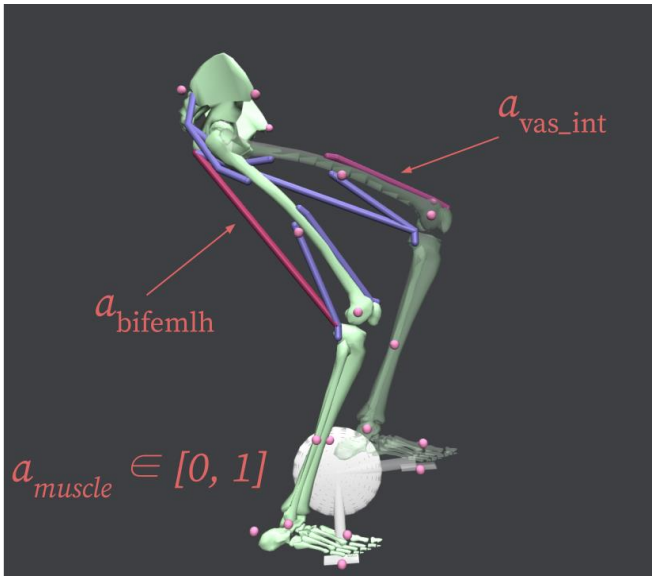

***Figure 6**, Computed Muscle Control (CMC) step. The CMC Tool generated a solution of muscle activations to produce the motion of the SFK Trial. To find a solution of muscle activations, an objective function containing the muscle activation values and deviations between desired joint angles and the CMC model joint angles was minimized. The labels show the changing activations of the vastus intermedius and the biceps femoris long head.*

The DOF that were tracked during the CMC simulation were the crank angle, hip angle, knee angle, and MTP angle. The crank angle was tracked for all trials to ensure a constant pedaling cadence of 80 RPM.

The CMC Tool simulation can be unstable in the sense that a solution of muscle activations may not always be found for the entire simulation window. Settings of the CMC Tool must be adjusted for each of the six different trials until convergence was achieved and a solution was determined for the entire simulation time of 0.75 seconds. We dealt with this obstacle by slightly adjusting the weighting of the reserve actuators of only the crank angle for each of the six CMC trials until a solution for the entire simulation time was found.

Once a CMC simulation was completed, the solved muscle activations were used to calculate the MEER of the muscles with OpenSim. The following section describes how we organized, plotted, and analyzed the data compiled in the workflow.

Organization of the Analysis

The results from our developed workflow were analyzed to not only show the results were reasonable, but also as a guideline for how to analyze the results of the developed computational workflow.

Analysis of Metabolic Energy Expenditure Rate (MEER)

The outputs of the CMC Tool trial step, muscle activations, were used to directly calculate MEER as a function of crank angle for each of the six trials analyzed. These six trials could then be compared in order to determine how MEER is affected by changes in saddle position.

An important step in MEER analysis was to average the MEER vs. crank angle over the entire cycle to obtain a full-cycle averaged MEER. This was important because the full-cycle averaged MEER captured the whole 0.75 second cycling gait cycle, and was a more stable value because it avoided numerical instability in the data from sharp MEER peaks. We summarized each of the six trials into six data points of full-cycle average MEER for direct comparison. This comparison of the six trials was best compared in a 3D bar plot, rather than a 3D surface plot, which would be a better visualization if a larger range of trials was analyzed.

We additionally plotted the MEERs for each of the muscles with respect to the crank angle. These plots were useful because they indicated when each of the muscles were activated during the pedaling motion. They also served to identify trends of how each muscle

was individually impacted by moving the saddle position.

Analysis of Muscle States

Muscle states analysis further validated our developed workflow to calculate MEER as a function of saddle position since muscle states can be analyzed for MEER insights, as explained in the Introduction. The muscle states outputs of the SFK step were used to calculate the active force capacity of muscle.

Using the relationships for the active force-length curve and force-velocity curve of muscle fibers as shown in **Figure 1** and **Figure 2**, we plotted the active force capacity of the model's muscles during the pedaling motion. Normalized fiber length and normalized fiber velocity are standard outputs for OpenSim simulations, and are exactly the required inputs for the active force function (recall **Equation (1)**). As mentioned previously, knowledge of the active force capacity of a muscle can be directly correlated to the MEER of that muscle. The active force plots we generated for the muscles were used to validate the MEER data computed using the CMC Tool. This analysis will be elaborated upon in the Results & Discussion section.

Pursuit of Wild Ideas

As we compiled and analyzed the results from our workflow, we decided on the level of complexity for our OpenSim model based on our goal to develop a workflow to understand the relationship between saddle position and MEER.

The inclusion of lower-leg muscles was the first course of action, in which we initially attempted to implement the gastrocnemius and tibialis anterior muscles for every SFK run within our workflow. We extracted the reaction forces at the pedal for this higher complexity model, but for each SFK run, this generated abnormally large reaction forces that were inconsistent with literature. Since these external forces were a direct input to the CMC Tool, as well, we were unable to generate reliable MEER results with consistent DOF constraints on the model. For this reason, the additional lower-leg muscles were omitted from the model used in our workflow for analysis of MEER and muscle states.

Additionally, we looked to expand our analysis to include a second leg in order to more accurately model the coupled motion between the two legs. Using our knowledge of the architecture of our single-leg model, we constructed a two-leg model that completed a SFK run with semi-realistic kinematics (**Appendix C**). While the toes' motion was not fully stable and the pelvis was not fully locked at the saddle position, this was a great accomplishment and the model can be utilized by Specialized.

Since our current cycling model did not account for resistance at the crank, we were also able to generate a proof-of-concept external force at the pedal in order to modulate the changing of gears, biking terrain, and internal bike geometries[45]. This will allow Specialized to more accurately model an individual's cycling motion for a plethora of scenarios.

The results in the next section focus on using the full workflow for the model described at the beginning of the Methods section. This model was selected to generate results because the motion of the leg and reaction forces at the pedal were of greatest fidelity when validated against literature[11][16][18][21].

Results & Discussion

Both the MEER results and muscle states results were used to validate the computational workflow we developed. The following plots show that our workflow can be used to generate data that is useful and interpretable. It is important to note that this workflow should be used for comparative studies across different trials of saddle positions, rather than absolute numerical analysis, as only one leg of the body is modeled and thus entire-body effects are not included.

CMC Results Analysis

The 3D Bar Plot for total full-cycle average MEER for all six CMC trials, **Figure 7**, showed a clear trend between saddle position and full-cycle averaged MEER. The saddle positions at R = 0.8196 m (θ = 102, 105, 108°) exhibited lower total full-cycle average MEER than the saddle positions at the larger radius, R= 0.8396 m (θ = 102, 105, 108°). This indicated that, for the smaller radius, the model's muscles required a lower MEER to reproduce the cycling motion, thus were more efficient.

The conclusions we drew from **Figure 7** are contrary to what has been stated in literature. The radius, R = 0.8396 m, was calculated from the inseam length of the model per the LeMond Method[25], as mentioned in the Methods section, for the ideal seat tube height from the bottom bracket. Thus, we expected any deviation from this seat post length (radius from the bottom bracket) would have resulted in a higher MEER. Instead, we observed that the saddle position with the smaller radius, which deviated from the ideal seat tube height by 2 cm, was more efficient.

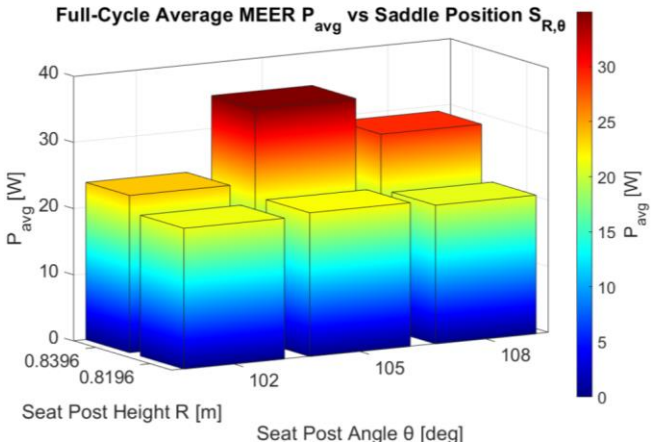

***Figure 7**, 3D Bar Plot for total full-cycle average MEER of all muscles for all six CMC trials. The total MEER across all muscles was averaged over the full 0.75 second simulation time to represent a MEER for each trial. Saddle position (R,θ) = (0.8396 m, 105°) produced the highest total full-cycle average MEER. Saddle position (R,θ) = (0.8196 m, 108°) produced the lowest total full-cycle average MEER.*

This discrepancy in results when compared to literature was reflected in not only the total MEER of all muscles, but also for each individual muscle's MEER over the full revolution cycle, as shown in **Figure 8**. However, we acknowledge that our result set was limited in that we only analyzed two distances (R) between the bottom bracket and the saddle.

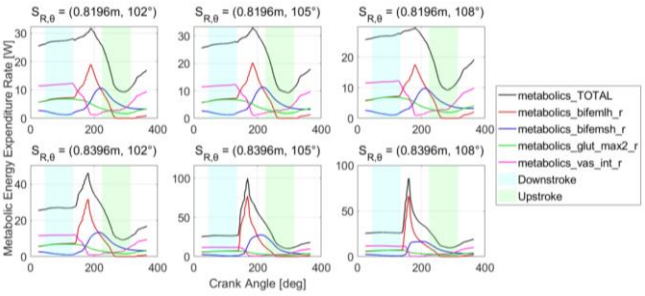

***Figure 8,** Metabolic Energy Expenditure Rates (MEER) for all 6 saddle positions. See **Appendix D** for a larger view. Saddle position radius varies by row and saddle position angle varies by column.*

We believe the differences in our MEER outputs compared to literature were due to the pedal forces that were extracted from the SFK step in our workflow and inputted into the CMC step of our workflow. As seen in **Figure 9**, the saddle positions at R = 0.8396 m had significantly higher pedal forces than the saddle positions at R = 0.8196 m. One potential source of force discrepancies may be due to the pedal clip constraint. It is possible that this constraint interacted unrealistically with the prescribed function at the crank and is an area for future investigation. This quadrupling of force was propagated through to the CMC step and to the MEER outputs shown in **Figure 8**.

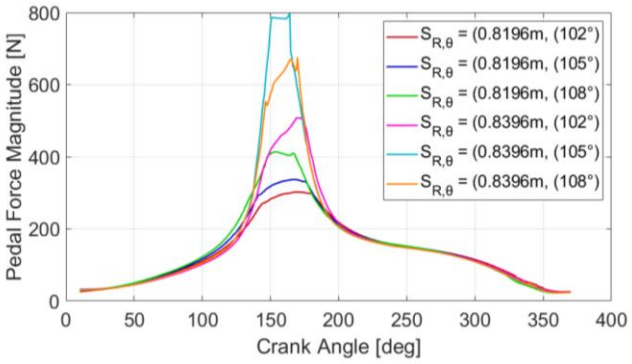

Figure 9. *Reaction pedal force magnitudes. Pedal force profiles on the midfoot for all six trials during SFK simulations. The forces peaked at the end of the downstroke at approximately 150° during the pedaling motion.*

Figure 10 showed the muscles' MEERs for one pedal cycle, which agreed with the expected muscle activation timings for all four muscles[11][16]. For example, looking at the results from the biceps femoris long head, the MEER during the downstroke and upstroke regions was lower, but in the transition between, the MEER increased significantly. This was in agreement with literature that noted the hamstring activates as it pulls the leg backwards in the transition from downstroke to upstroke[11][16]. The MEER for other muscles can be similarly validated. The vastus intermedius activation peaked in the downstroke, which is representative of the force exerted by the quadricep while pushing down on the pedal during downstroke. The activation for the vastus intermedius rose again in the upstroke due to the activation needed when sweeping the leg forward through the end of the upstroke region. The biceps femoris short head exhibited trends that were also consistent with literature; it worked in tandem to flex the knee joint with the biceps femoris long head, another hamstring muscle. Finally, the gluteus maximus muscle activated to extend the hip joint during the downstroke and tapered off in the upstroke. All four muscles' activations exhibited trends consistent with literature of cycling motion muscle activation[11][16].

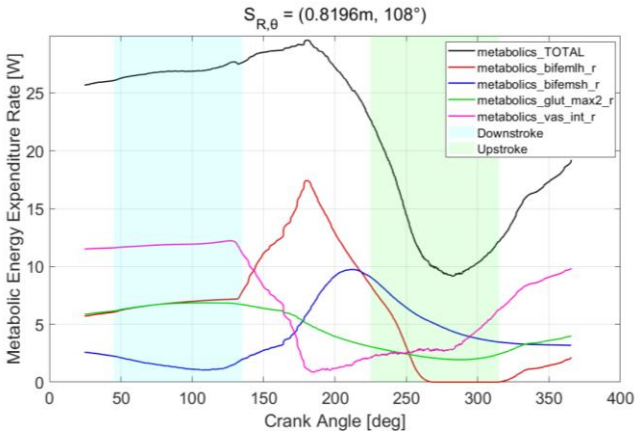

Figure 10*, Metabolic Energy Expenditure Rates (MEER) for all muscles for saddle position (R, θ) = (0.8196 m, 108°) in which total full-cycle average MEER was lowest for all trials analyzed. MEER for biceps femoris long head (red), biceps femoris short head (blue), gluteus maximus (green), vastus intermedius (pink) were plotted against crank angle for one revolution. The total MEER across all muscles (black) was also plotted. The shaded blue region corresponds to the downstroke of the cycling motion, and the shaded green region corresponds to the upstroke.*

Muscle States Analysis

Muscle states analysis was performed to validate cycling dynamics as well as validate MEER outputs. By looking at the relative trends between saddle positions' active force capacities, insights about the relative differences in MEER could also be determined.

Active force capacity plots for all six saddle positions were generated, as seen in **Figure 11**. The active force capacity was calculated as mentioned in the Methods section. In these plots, we observed that the relative muscle trends were consistent across all six saddle positions. In the saddle positions at the longer radius (R = 0.8396 m), we can see that the peak active force capacities of the vastus intermedius were generally larger than the peak active force capacities of the vastus at the shorter saddle position radius (R = 0.8196 m), as shown in **Figure 11**.

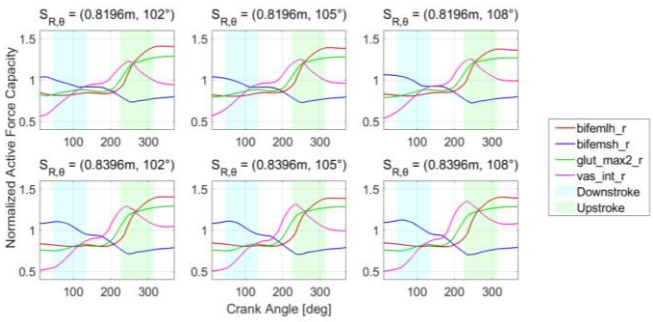

Figure 11, *Normalized Active Force Capacities for all 6 saddle positions, calculated from the Simulated Forward Kinematics (SFK) muscle states outputs for each saddle position. See* ***Appendix D*** *for a larger view.*

To understand how the individual muscle active force capacities helped validate our workflow, we can look at just one saddle position (R = 0.8196 m, θ = 108°). **Figure 12** showed that the active force capacity trends we observed corresponded to literature findings on fiber length and fiber velocity trends[21]. Specifically, we saw that the biceps femoris long head force peaked at maximum eccentric contraction at a crank angle of ~300°. Eccentric contraction is when the muscle elongates and performs negative work. This corresponded well to our understanding of cycling motion as in the tail end of the upstroke, the knee extends which allows the biceps femoris long head to contract eccentrically. Looking at the vastus intermedius muscle in **Figure 12,** we saw that its active force capacity peaked at the beginning of the upstroke region. This is because this muscle's fiber length was longest at this point in a cycling motion. In summary, the active force capacity for each muscle validated the workflow's SFK step's ability to generate realistic motion.

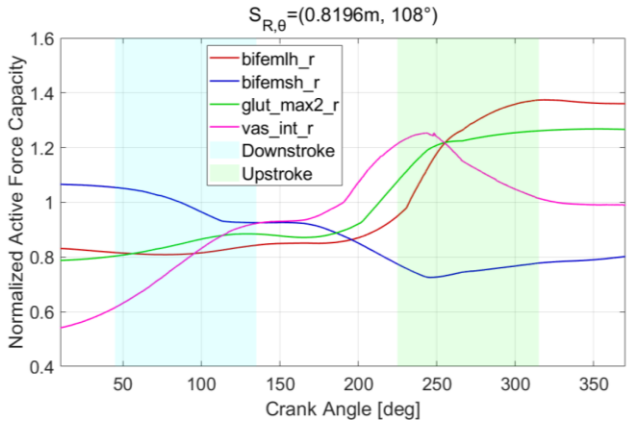

Figure 12, *Normalized Active Force Capacities for saddle position (R, θ) = (0.8196 m, 108°), calculated from the muscle states outputs.*

The active force capacity plots from muscle states were also used to validate the MEER results. This can be observed in **Figure 13**, which showed the MEER for the vastus intermedius at three saddle positions: (R,θ) = (0.8196 m, 102°), (0.8196 m, 105°), and (0.8196 m, 108°). The vastus intermedius at seat angle of θ = 102° had the lowest active force capacity which was particularly noticeable at a crank angle of ~250°. At a lower active force capacity, this particular position would require a higher activation of the vastus intermedius muscle in order to see that same force output. This is confirmed by the MEER of the vastus intermedius plotted for the three saddle positions: (R,θ) = (0.8196 m, 102°), (0.8196 m, 105°), and (0.8196 m, 108°) as seen in **Figure 14** in which the MEER for saddle position (R,θ) = (0.8196 m, 102°) was largest. Thus, the muscle's MEER was largest for the saddle position with the lowest active force capacity.

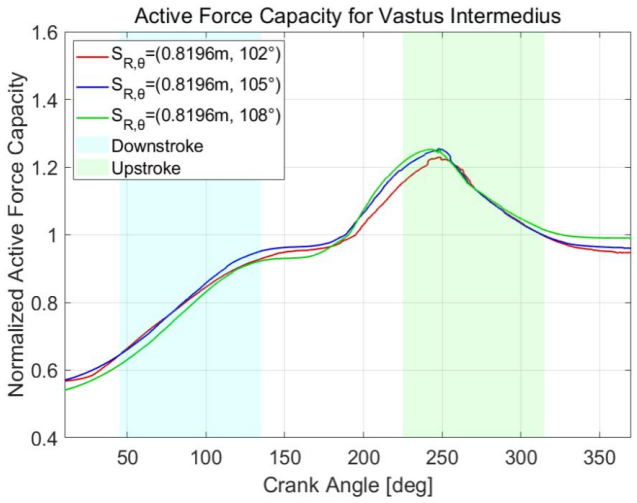

Figure 13, *Normalized Active Force Capacities for saddle position (R, θ) = (0.8196 m, 108°). Force for biceps femoris long head (red), biceps femoris short head (blue), gluteus maximus (green), vastus intermedius (pink) were plotted against crank angle for one revolution. The shaded blue region corresponds to the downstroke of the cycling motion, and the shaded green region corresponds to the upstroke.*

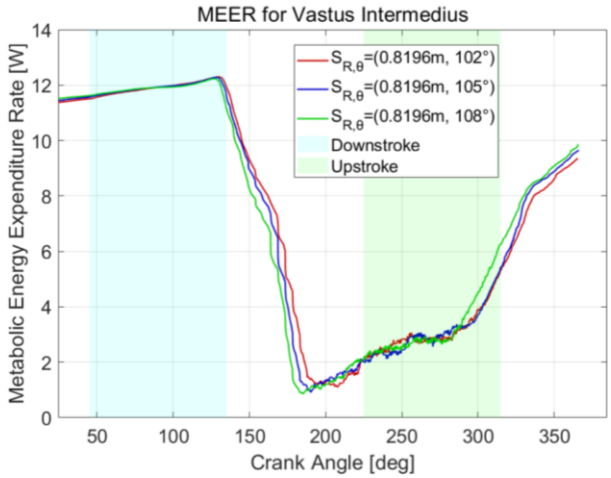

Figure 14, *Normalized Active Force Capacities for the Vastus intermedius at 3 saddle positions: (R,θ) = (0.8196 m, 102˚), (0.8196 m, 105˚), and (0.8196 m, 108˚). Force for biceps femoris long head (red), biceps femoris short head (blue), gluteus maximus (green), vastus intermedius (pink) were plotted against crank angle for one revolution. The shaded blue region corresponds to the downstroke of the cycling motion, and the shaded green region corresponds to the upstroke.*

From the results, we showed that the workflow we created was capable of producing MEER results that are realistic when being used to compare against other saddle positions. Furthermore, we showed that the muscle states obtained from the SFK step can be used to validate the model's motion as well as the MEER insights.

Conclusion

Conclusions from the Analyzed Results of the Workflow

In summary, our results showed that MEER was more sensitive to saddle position radius than saddle position angle, with the smaller radius (R = 0.8196) and largest angle (θ = 108˚) achieving the lowest MEER. The discrepancy of these results compared to literature[25] were likely due to high peaks seen in the pedal reaction forces. More importantly, visualization and validation of muscle activation times through MEER outputs confirmed this workflow's ability to generate realistic insights that can be used for relative saddle position comparison.

Muscle states were an intermediate output in our workflow and were obtained from running the SFK step. The normalization and multiplication of the force length and force velocity curves (**Equation (1)** of the Introduction) can give information about active muscle force capacity. Higher active force capacity magnitudes would be expected to correspond to lower MEER[22][23][24] and vice versa. This is what we observed in our results. These muscle states served as a verification check for CMC MEER outputs and can also be used standalone for implicit MEER analysis. If used standalone, the muscle states analysis has the potential to generate insights through quick and repeatable iterations over a wide range of saddle positions without the need for the CMC step. This may be an important heuristic for Specialized moving forward as muscle states analysis determines active force capacity trends, and thus MEER trends, without

calculating MEER through the complicated and time-consuming CMC Tool.

Ideas for Future Work

Using the findings described throughout this report, Specialized now has the tools and capabilities to explore cycling MEER in more detail than ever before. Looking beyond the scope of this 10-week project, Specialized may validate the results of the model with experimental data. This can be achieved through experimental motion capture data of joint angles and experimental pedal reaction forces. Furthermore, Specialized can correlate their lab's EMG results in order to verify the muscle activations of the cycling model. We heavily relied on literature to justify the trends observed in our analyses, but Specialized can utilize their network of cycling performance specialists to further validate the model. Moreover, Specialized may choose to further pursue the directions we described in the Pursuit of Wild Ideas subsection.

Overall Conclusions of the Developed Computational Workflow

Overall, we developed a computational workflow to relate cyclist MEER to saddle position. Using the workflow, we generated and analyzed the results to show confirmation that the workflow can be implemented. We used this workflow for a set of six saddle positions and analyzed the results. With an input of saddle position, the workflow used OpenSim modeling to establish the relationship between changes in saddle position and MEER. The results showed a clear indication of which saddle position had the lowest full-cycle averaged MEER. MEER was also analyzed for each muscle, allowing for a deeper understanding of the total MEER for each saddle position. Furthermore, muscle states analysis for active force capacity proved useful for our workflow objectives both as a validation step for the MEER and as a standalone analysis method.

This computational workflow method was created to be used in the place of time-consuming traditional sports performance analysis methods with experimental data collection, often done in research, but unrealistic for quick-turn industrial design cycles. The developed computational workflow leveraged OpenSim modeling and tools to calculate MEER in order to determine the relationship between changes in saddle position and MEER. This workflow method may now be used by our industry sponsor, Specialized, in their bicycle design cycle.

References

[1] Tucker, JT. (11 January 2021). Specialized ME319 Collaboration Kickoff Presentation.

[2] Faulkner, S. and Jobling, P. *The Effect of Upper-Body Positioning on the Aerodynamic-Physiological Economy of Time-Trial Cycling.* International Journal of Sports Physiology and Performance, (2020).

[3] Dodge, David. *The Most Efficient Transportation On the Planet*. Huffington Post Online (2013).

[4] Koelewign, A. D. et al. *Metabolic cost calculations of gait using musculoskeletal energy models, a comparison study.* PLOS ONE 14(9): e0222037, (2019).

[5] Dembia CL, Silder A, Uchida TK, Hicks JL, Delp SL *Simulating ideal assistive devices to reduce the metabolic cost of walking with heavy loads.* PLOS ONE 12(7): e0180320, (2017).

[6] Jackson, R. W. and Collins, S. H. *An experimental comparison of the relative benefits of work and torque assistance in ankle exoskeletons*. J Appl Physiol 119: 541–557, (2015).

[7] Leib, D. *The Effects of Cleat Placement on Muscle Mechanics and Metabolic Efficiency in Prolonged Sub-Maximal Cycling*. Ball State University Biomechanics Laboratory Thesis, (2008).

[8] Pottinger, M. *Inverse Dynamic Analysis of ACL Reconstructed Knee Joint Biomechanics During Gait and Cycling Using OpenSim*. California Polytechnic State University, San Luis Obispo Thesis, (2018).

[9] Coleman DA, Wiles JD, Davison RC, Smith MF, Swaine IL. *Power output measurement during treadmill cycling*. Int J Sports Med. ;28(6):525-30, (2007).

[10] Peveler, W. and Green, J. Effects Of Saddle Height On Economy And Anaerobic Power In Well-trained Cyclists. National Strength and Conditioning Association , Vol 25, 3, (2011).

[11] Hull, M.L. and Jorge, M. *A Method For Biomechanical Analysis of Bicycle Pedalling*. Journal of Biomechanics Vol 18 No 9. pp 631-644, (1985).

[12] Gonzalez, H. and Hull, M.L. *Multivariable Optimization of Cycling Biomechanics*. Journal of Biomechanics Vol. 22 No 11/12 pp 1151-1161, (1989).

[13] Uchida TK, Seth A, Pouya S, Dembia CL, Hicks JL, Delp SL (2016) *Simulating Ideal Assistive Devices to Reduce the Metabolic Cost of Running*. PLoS ONE 11

[14] Uchida TK, Hicks JL, Dembia CL, Delp SL (2016) *Stretching Your Energetic Budget: How Tendon Compliance Affects the Metabolic Cost of Running*. PLoS ONE 11

[15] Hamner, Samuel R, Delp, Scott L. *Muscle contributions to fore-aft and vertical body mass center accelerations over a range of running speeds*, Journal of Biomechanics, Volume 46, Issue 4, 2013

[16] Fonda, B., & Sarabon, N. (2010). *Biomechanics of cycling (Literature review)*. Sport Science Review, 19(1), 187–210

[17] Ferrer-Roca V, Roig A, Galilea P, García-López J. *Influence of saddle height on lower limb kinematics in well-trained cyclists: static vs. dynamic evaluation in bike fitting*. J Strength Cond Res. 2012

[18] Bini RR, Tamborindeguy AC, Mota CB. *Effects of saddle height, pedaling cadence, and workload*

on joint kinetics and kinematics during cycling. J Sport Rehabil. 2010

[19] Henrot, C and Jeffries, L. *OpenSim Teaching Materials -- Educational Cycling Model*. BIOE-ME 485 Spring 2018

[20]*OpenSim::Umberger2010MuscleMetabolicsProbe Class Reference*. OpenSim API 3.3 Documentation (2015).

[21] Uchida, Thomas K., et al. Biomechanics of Movement: The Science of Sports, Robotics, and Rehabilitation. The MIT Press, 2021.

[22] Bohm Sebastian, Mersmann Falk, Santuz Alessandro, and Arampatzis Adamantios (2019) *The force–length–velocity potential of the human soleus muscle is related to the energetic cost of running* Proc. R. Soc. B.286

[23] Alcazar J, Csapo R, Ara I and Alegre LM (2019) *On the Shape of the Force-Velocity Relationship in Skeletal Muscles: The Linear, the Hyperbolic, and the Double-Hyperbolic.*

[24] Umberger, Brian R., Karin G.M. Gerritsen & Philip E. Martin (2003) *A Model Of Human Muscle Energy Expenditure, Computer Methods In Biomechanics And Biomedical Engineering,*

[25] Bini, Rodrigo & Hume, Patria & Croft, James. (2011). Effects of Bicycle Saddle Height on Knee Injury Risk and Cycling Performance. Sports medicine (Auckland, N.Z.). 41. 463-76. 10.2165/11588740-000000000-00000.

[26] Wozniak Timmer, Cheryl A., MS, PT. (1991). Cycling Biomechanics: A Literature Review. Journal of Orthopaedic & Sports Physical Therapy. 14:3. 106-113.

[27] Quintana-Duque, J.C., Dahmen, T., Saupe, D., 2015. *Estimation of torque variation from pedal motion in cycling*. Int. J. Comput. Sci. Sport 14, 34–50.

[28] Pappas, E (2019) *Do Female Athletes get ACL injuries because of their ANATOMY?*

[29] Gaesser GA, Brooks GA. Muscular efficiency during steady-rate exercise: effects of speed and work rate. J Appl Physiol. 1975 Jun;38(6):1132-9. doi: 10.1152/jappl.1975.38.6.1132. PMID: 1141128.

[30] CHOOSING BIKE TYPE. 2018. Recycled Cycles & Service. St. Louis, MO. http://www.recycledcycles.net/type1.html

[31] Kitawaki, Tomoki & Oka, H.. (2013). A measurement system for the bicycle crank angle using a wireless motion sensor attached to the crank arm. J Sci Cycling. Vol. 2(2), 13-19

[32] Wilkinson, R. (10 March 2021). Personal Correspondence via E-mail.

[33] Umberger BR, Gerritsen KG, Martin PE. Muscle fiber type effects on energetically optimal cadences in cycling. J Biomech. 2006;39(8):1472-9. doi: 10.1016/j.jbiomech.2005.03.025. Epub 2005 May 31. PMID: 15923008.

[34] *SimTK::Assembler Class Reference*. OpenSim Simbody 3.5 Documentation (2016). https://simbody.github.io/3.5.0/classSimTK_1_1Assembler.html

[35] *OpenSim::AssemblySolver Class Reference*. OpenSim API 4.1 Documentation (2020). https://simtk.org/api_docs/opensim/api_docs/classOpenSim_1_1AssemblySolver.html

[36] Tucker, JT. (12 March 2021). Week 9 Update Presentation

[37] Ong, C. (10 March 2021). Week 9 Correspondence.

[38] Uchida, T.K., Sherman, M., and Dembia, C. Simbody Assembler.cpp SimTK Open Source Simbody GitHub Repository. (24 July, 2017)

https://github.com/simbody/simbody/blob/master/Simbody/src/Assembler.cpp#L754

[39] Carbonetto, P., Schmidt, M., and de Freitas, Nando. (2008) An interior-point stochastic approximation method and an L1-regularized delta rule. Advances in Neural Information Processing Systems (NIPS) Conference. Department of Computer Science, University of British Columbia Vancouver, B.C., Canada.

[40] Tsianos GA, MacFadden LN. Validated Predictions of Metabolic Energy Consumption for Submaximal Effort Movement. PLoS Comput Biol. 2016;12(6):e1004911. Published 2016 Jun 1. doi:10.1371/journal.pcbi.1004911

[41] "Getting Started with Forward Dynamics." OpenSim Documentation. https://simtk-confluence.stanford.edu/display/OpenSim/Getting+Started+with+Forward+Dynamics

[42] "Getting Started with CMC." OpenSim Documentation. https://simtk-confluence.stanford.edu/display/OpenSim/Getting+Started+with+CMC

[43] "OpenSim::Thelen2003Muscle Class Reference." OpenSim API 4.1 (2020). https://simtk.org/api_docs/opensim/api_docs/classOpenSim_1_1Thelen2003Muscle.html

[44] "Thelen2003Muscle.cpp" OpenSim Actuators GitHub Open Source Code Documentation. https://github.com/opensim-org/opensim-core/blob/master/OpenSim/Actuators/Thelen2003Muscle.cpp

[45] Quintana-Duque, Juan Carlos, Thorsten DAHMEN, Dietmar SAUPE, 2015. Estimation of Torque Variation from Pedal Motion in Cycling. In: International Journal of Computer Science in Sport. 14(1), pp. 34-50. eISSN 1684-4769

[46] Duggan, W., Donne, B., & Fleming, N. (2017). Effect of Seat Tube Angle and Exercise Intensity on Muscle Activity Patterns in Cyclists. International journal of exercise science, 10(8), 1145–1156.

Appendix A: DOF

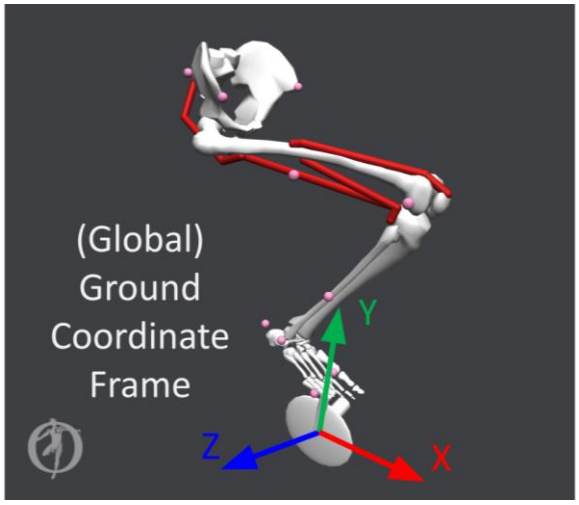

Figure A.1, Ground Coordinate Frame. The global ground coordinate frame was centered at the location of the bottom bracket.

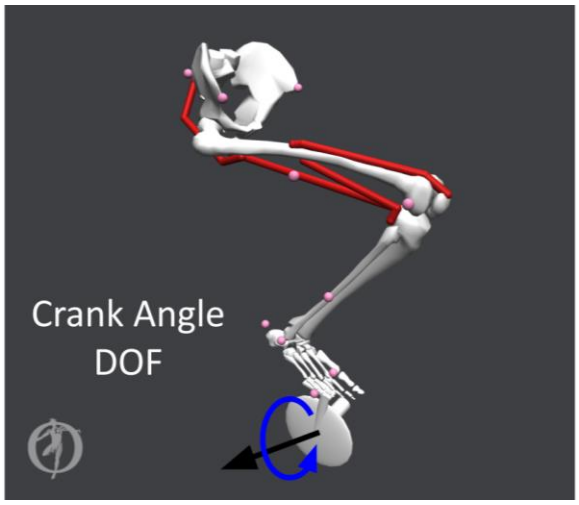

Figure A.2, Crank Angle DOF. Crank angle rotation (rotation in blue).

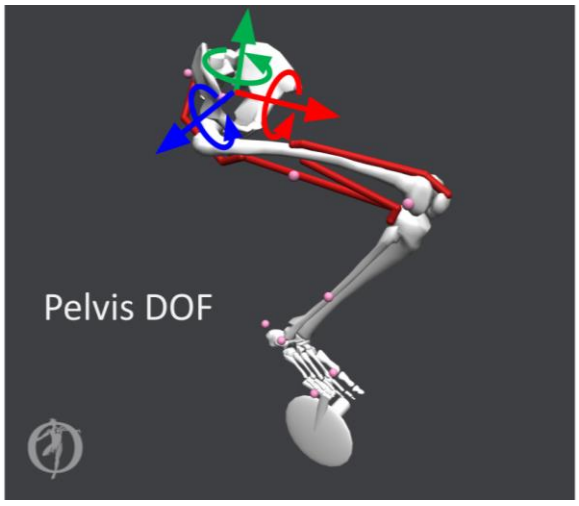

Figure A.3, Pelvis DOF. Pelvis translational x-axis (red axis), pelvis translational y-axis (green axis), pelvis translational z-axis (blue axis), pelvis list angle (rotation about red axis), pelvis rotation angle (rotation about green axis), and pelvis tilt angle (rotation about blue axis).

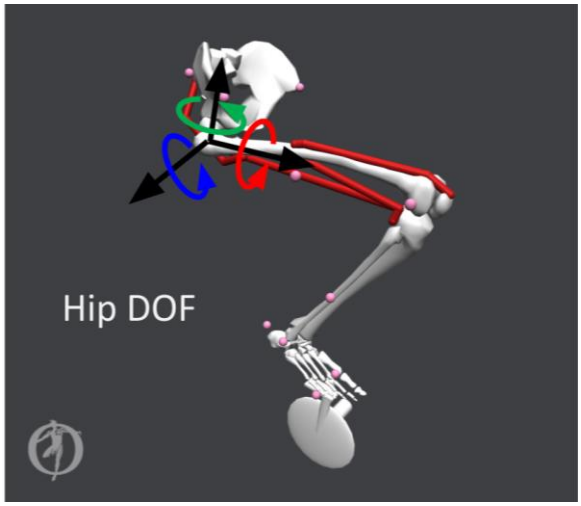

Figure A.4, Hip DOF. Hip adduction angle (rotation in red), hip rotation angle (rotation in green), and hip angle (rotation in blue).

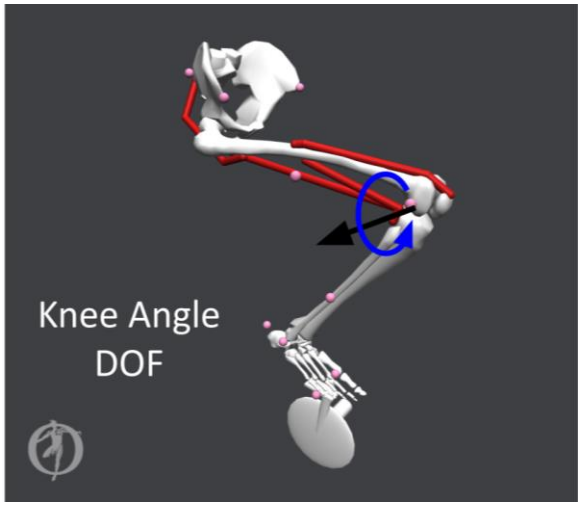

Figure A.5, Knee Angle DOF. Knee angle rotation (rotation in blue).

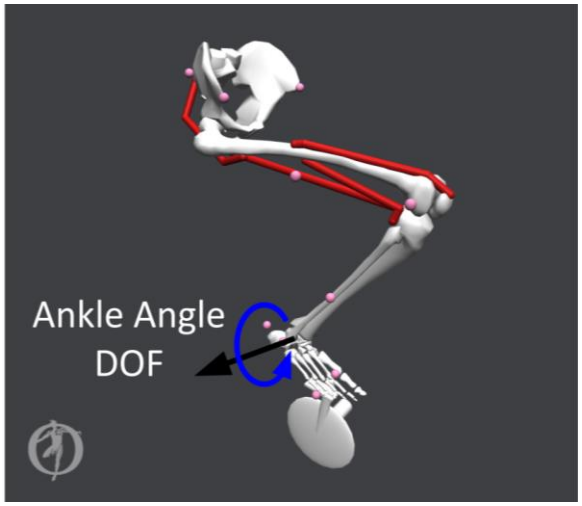

Figure A.6, Ankle Angle DOF. Ankle angle rotation (rotation in blue).

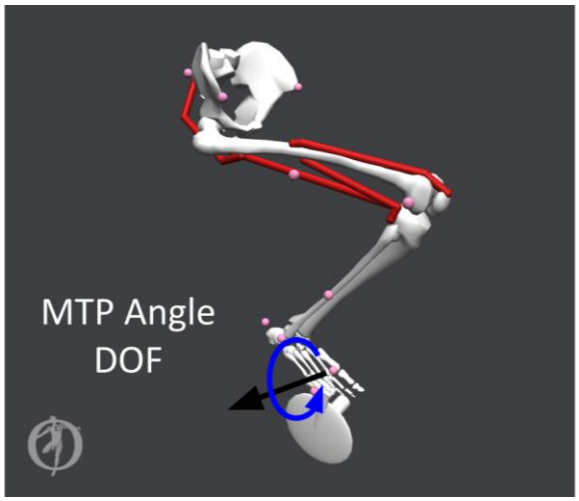

Figure A.7, Metatarsophalangeal (MTP) Angle DOF. Metatarsophalangeal angle rotation (rotation in blue).

Appendix B: OpenSim Assembly Optimization (Multibody solver)

OpenSim's Assembly solver handled the construction of the model with new coordinates at every time step with optimization of an objective function, *A*. The objective function was equal to the squared error between the current timestep's model coordinates and the desired model coordinates, and was minimized to determine the new position of the model. The objective function is defined in **Equation (3)** [35]:

$$A = \Sigma(w_i\,(q_i - q_{des,\,i})^2)$$
$$A \text{ subject to constraint equations: } G(q)\text{-}G_0 = 0 \qquad \textbf{(3)}$$

q_i = *coordinate value for upcoming time step*
$q_{des,i}$ = *coordinate value that currently satisfies constraints*
w_i = *weights on coordinates*
$G(q)\text{-}G_0$ = *holonomic constraints on coordinates*

The desired coordinates were chosen to be near the current state of the model. This ensured the optimizer's likelihood of converging to a solution. This process is deterministic for stable initial conditions and simple constraints, as the solution of coordinates given by the Forward Dynamics Tool and the Assembly solver can be consistently reproduced. This is because the OpenSim Assembly solver source code[38] uses the interior point methods optimization for constrained problems which is not stochastic[38] [39].

Appendix C: 2-Leg Model

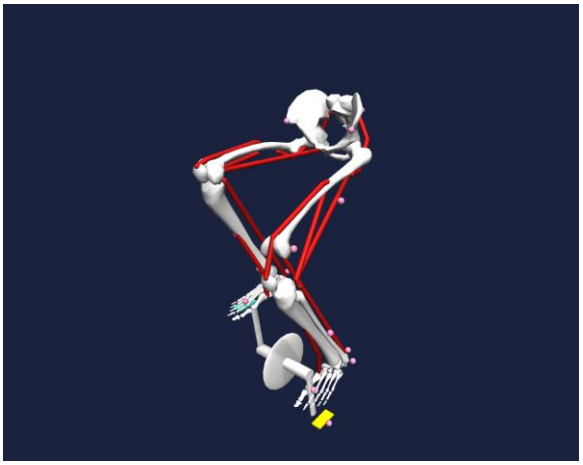

Figure C.1, Two-Leg Model. Fully-assembled two-leg model for which a SFK run was completed.

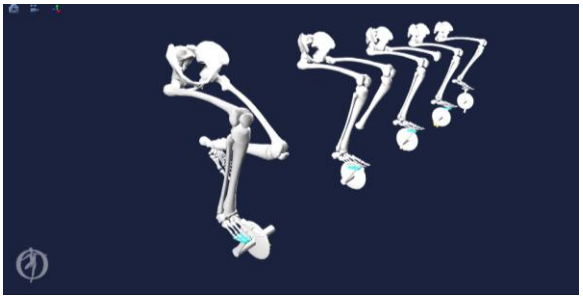

Figure C.2, Two-Leg Model Progression. Construction of two-leg model from scratch, while incorporating necessary constraints and degrees of freedom.

Appendix D: Enlarged View of Results

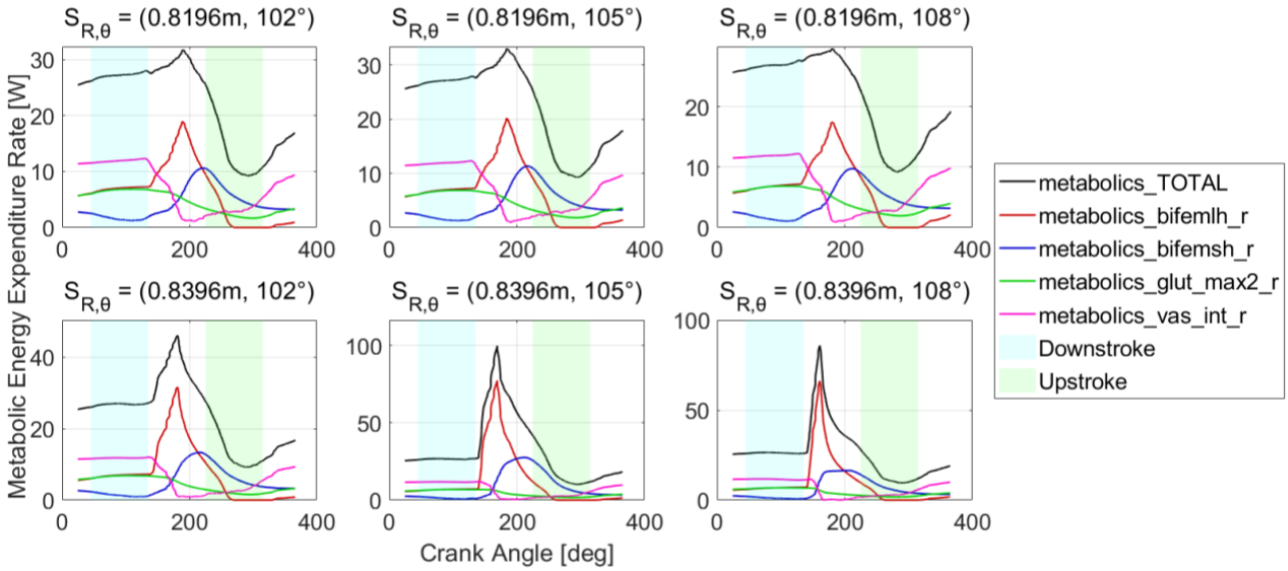

Figure D.1. Metabolic Energy Expenditure Rates (MEER) for all 6 saddle positions. Saddle position radius varies by row and saddle position angle varies by column. The shaded blue region corresponds to the downstroke of the cycling motion, and the shaded green region corresponds to the upstroke.

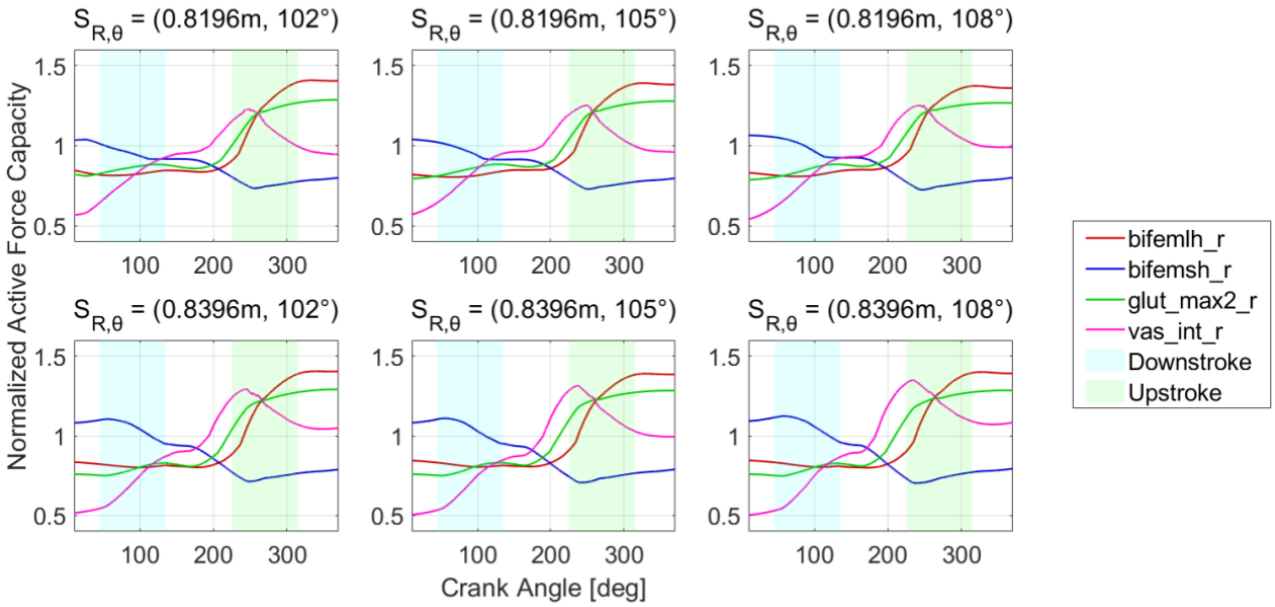

Figure D.2. Normalized Active Force Capacities for all 6 saddle positions, calculated from the muscle states outputs for each saddle position. The shaded blue region corresponds to the downstroke of the cycling motion, and the shaded green region corresponds to the upstroke.